Analytical modeling of no-load eccentric slotted surface mounted PM machines: cogging torque and radial force

Samad Taghipour Boroujeni[1], Pezhman Jalali[1], and Nicola Bianchi[2], *Fellow, IEEE*

[1] Engineering Department, Shahrekord University, Shahrekord, Iran
[2]Industrial Engineering Department of Padua University, Padua, Italy

In this work the air gap flux density components in the eccentric surface-mounted PM machines are predicted analytically. In the provided model the slotting effects of the armature are taken into account. In the modeling process, Conformal Transformations (CTs) are employed to obtain an equivalent concentric slotless machine for the eccentric slotted PM machine. To satisfy the condition of using CTs, i.e. having a Laplace equation, the PMs are replaced with an equivalent current sheet at the surface of the rotor. The approach of finding this current sheet is approved by the basis of the Electromagnetic theory. One of the contributions of this work is that, the provided model is capable of modeling the eccentric surface-mounted PM machines with any PM magnetization pattern by means of CTs. Substituting, the predicted air gap flux density components in the Maxwell stress tensor, the machine unbalanced magnetic force and its cogging torque is computed. Finally, the accuracy of the obtained results is evaluated by means of Finite Element Analysis.

***Index Terms*— Analytical modeling, cogging torque, conformal transformation, eccentricity, equivalent current sheet, slotted armature, unbalanced magnetic force**

I. Introduction

The Surface-mounted PM (SPM) machines have a lot of merits such as the brushless and compact structure, easy control and long maintenance period. However, they suffer from the torque pulsation. This pulsation is mainly due to the machine cogging torque. In addition, inaccuracies in assembling of the SPM machines results in the rotor eccentricity which causes in a high level of Unbalanced Magnetic Force (UMF). It is well-known that, cogging torque [1] and UMF [2], [3] are the main sources of vibration and acoustic noise in the SPM machines [4], [5]. Here, in this work an analytical model is developed for computation of cogging torque and UMF in the eccentric SPM machines.

Computation of the cogging torque in SPM machines is one of the main concerns of the machine designer. Analytical approaches for the calculation of cogging torque have some advantages over the numerical methods. Although numerical methods such as Finite Element Analysis (FEA) are exact, they are time-consuming and sensitive to the appropriate mesh generation. Cogging torque could be computed by the methods such as, derivation of the magnetic energy variation [1], Maxwell stress tensor [6], integration of the magnetic stress vector along the slot sides [7] and Lorentz equation [8]. However, knowing the exact distribution of the air gap flux density components is an important prerequisite of the mentioned methods. In all of these methods, cogging torque is highly sensitive to the accuracy of the computed air gap flux density components. The proposed analytical approaches for modeling of the flux density in a slotted air gap could be categorized in three main groups as Sub-domain Analysis Methods (SAM) [9], Conformal Mapping Methods (CMM) [6], [7], [10] and Equivalent Magnetization Current (EMC) methods [8], [11]. Although SAMs have a very good accuracy, they need solving of linear Cramer equations. CMMs are basically applicable only in the problems with the Laplace equation [12]. However, in [6] and [7] CMMs are applied on the Poisson equation. The precision of the obtained results for the cogging torque by [6] and [7] includes some major and minor tolerances, respectively. In fact, the PM deformation is a concern in CMM, which is not considered in [6] and [7]. In addition, the impact of the slots on each other is missed in [6]. In the EMC method, it is necessary to apply a combined analytical-iterative algorithm to compute the air gap flux density in the slotted air gap [8], [11]. A nice comparison between different approaches of cogging torque computation is reported in [13].

In the case of having a rotor eccentricity in the SPM machine, computation of the air gap flux density is more cumbersome. There are few papers addressing analytical computation of the air gap flux density components in the eccentric slotted SPM machines [14]-[25]. In [14], [15], SAM is combined with the Perturbation Analysis (PA) method to predict the air gap flux density in the slotted SPM machines. In [15]-[17], cogging torque in the eccentric SPM machine is computed by PA method. In [17], the impact of the magnet imperfection and its magnetization pattern on the cogging torque of the eccentric SPM machine is studied. Although the accuracy of the PA is acceptable, it is restricted by the model order (zero and first). In addition, the PA method includes complex mathematical expressions and consequently, it increases the difficulty of the modeling process when combined with SAM. In a different way from the mentioned researches, in [18], the no-load air gap flux density of an eccentric SPM machine is computed by superposition of air gap flux densities of some concentric SPM machines with

Manuscript received April 1, 2015; revised May 15, 2015 and June 1, 2015; accepted July 1, 2015. Date of publication July 10, 2015; date of current version July 31, 2015. Corresponding author: S. T. Boroujeni (e-mail: s.taghipour@eng.sku.ac.ir).

Color versions of one or more of the figures in this paper are available online at http://ieeexplore.ieee.org.

Digital Object Identifier (inserted by IEEE).

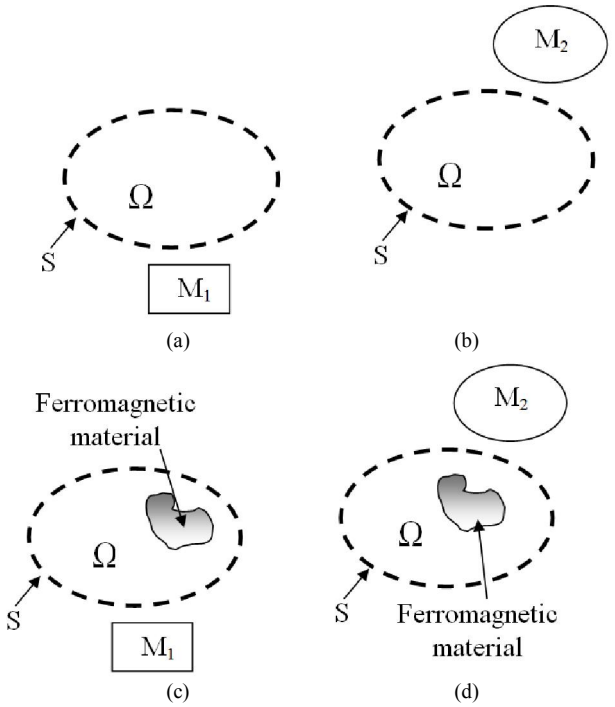

Fig. 1. (a) Two magnetic sources M_1 and M_2 cause the same magnetic flux density in the free space. (b) a ferromagnetic material is considered in Ω_2

different air gap lengths. However, the machine cogging torque is not computed and no mathematical approval is presented in [18]. The CMM is applied in for modeling and analysis of slotted eccentric radial flux [19], [20] and axial flux PM machines [21] and [22]. However, the limitation of applying CMMs on the Poisson equation is still a problem. The predicted components of the air gap flux density in [20] include some content of error which could be resulted in a high-level of inaccuracy in the cogging torque and UMF computation. The proposed methods in [21]-[22], pursue the developed models in [6] and [7] for the eccentric radial flux PM machines. They apply the Schwartz-Cristofell and bilinear transformations to compute the relative complex permeability of the eccentric air gap. Although the CMMs are applied on the Poisson equation, the predicted results by the quasi 3D models in [21], [22] are precise. Efficient and simple models based on the Equivalent Surface Current (ESC) are presented in [23], [24] for modeling of eccentric and slotless SPM machines with and without using Conformal Transformations (CTs), respectively. The methods in [23] and [24] are not capable modeling of the slotted stator. Against [23] and [24] that the eccentric stator is replaced by ESC, in this paper the stator is not changed and the PMs of the rotor are replaced by an ESC. This trick helps to consider any geometry for the stator slots and makes using the other field analysis methods such as SAM or CMM very easy.

In the presented work, the air gap flux density components are predicted in the eccentric surface-mounted PM machines. In the provided model the slotting effect of the armature is taken into account accurately. In the modeling process, CTs are employed to obtain an equivalent concentric slotless machine for the eccentric slotted one. In addition to satisfy the condition of using the CTs, i.e. having the Laplace equation, the PMs are replaced with an ESC at the surface of the rotor. The approach of finding this current sheet is approved on the basis of the Electromagnetic theory. The provided model is capable of modeling the eccentric slotted SPM machines with any PM magnetization pattern by means of CMM. Hereafter, the assumptions and the modeling procedure are presented in the section II. Two hypotheses are presented and approved in section II. In section III, the model is described. In this section, the used CTs are introduced and the air gap flux density components in the eccentric slotted SPM machine are obtained analytically. In addition, by using the Maxwell stress tensor, the machine UMF and its cogging torque are computed. Finally, the accuracy of the obtained results is evaluated by means of FEA in IV.

II. Basis of the Work

In this section the assumptions, the work procedure and the perquisites of the modeling process are briefly presented.

A. Assumptions

The following assumptions are made in the modeling process of the slotted eccentric SPM machine.

- Magnetic saturation is neglected.
- A unit value is considered for the relative permeability of the PMs.
- End effects are not considered.
- The stator is slotted and it is open-circuit.
- The provided MATLAB toolbox in [26] is used to apply the needed Schwartz-Christofell transformation.

B. Hypotheses

In this section, two hypotheses H_1 and H_2, are presented and approved. These hypotheses will be used in computation of the ESC. In Fig.1 (a) and (b) the magnetic sources, M_1 and M_2, are considered respectively, outside the closed surface S. The surface S encircles the volume Ω. It is assumed that there is free space in the volume Ω. Based on the uniqueness theorem in Electromagnetics, it is claimed that:

H_1: If the same tangential field is caused by the sources M_1 and M_2 in Fig.1 (a) and (b) at S, then the field distributions in the points of Ω in Fig.1 (a) and (b) are the same [27].

H_2: It is assumed that the magnetic sources M_1 and M_2 in the Fig.1 (a) and (b) cause the same field distributions inside Ω. In this condition, if any ferromagnetic body with an arbitrary shape is inserted in the volume Ω, see Fig. 1 (c) and (d), again the field distributions in the volume Ω in Fig.1 (c) and (d) are the same. This hypothesis could be approved by using the concept of Magnetization Surface Currents (MSC). From the Electromagnetic theory, each ferromagnetic material could be replaced by the free space, some MSC on the surface of the material and some Magnetization Volume Current (MVC) in the points inside of the material body [27]. If the permeability of the ferromagnetic material is infinite the MVC is zero and the MSC nullifies the tangential flux density at the surface of the material [11]. Since, there is the same flux density distribution in Ω in Fig.1 (a) and (b), after adding the ferromagnetic material, respectively in Fig.1 (c) and (d), the

same MSC is needed to nullify the tangential flux density at the surface of the ferromagnetic material by M_1 and M_2 in Fig.1 (c) and (d). Therefore, based on the superposition theorem an identical field distribution in Ω will be obtained in Fig.1 (c) and (d). In other words, if the magnetic flux density in the volume Ω caused by M_1 and M_2 in Fig.1 (c) and (d) are equal for one ferromagnetic material, this equality is valid for other shapes of the ferromagnetic materials.

It is useful to apply H_1 to equalize the PMs of a slotless concentric SPM machine with an ESC on its rotor surface as shown in Fig.2 (a) and (b), respectively. Let us consider the PMs in Fig.1 (a) and the ESC in Fig.2 (b) as the magnetic sources M_1 and M_2, respectively, and selecting the region Ω as $R_m<r$. The curve S is expressed as $r=R_m$, where R_m is the PM radius. Therefore, if the same tangential fields is generated at $r=R_m$ in Fig.2 (a) by PMs and in Fig.2 (b) by ESC, the same field is obtained in $R_m<r$ in Fig.2 (a) and (b). In this step the slotless concentric stator is removed and replaced with another ferromagnetic material, i.e., a slotted eccentric one. Since the PMs and ECS are equal together, based on H_2, it could be claimed that the magnetic flux density for $R_m<r$ in Fig.2 (c) and (d) are the same.

C. Modeling procedure

In the proposed modeling process, the following steps are carried out to find the air gap flux density components in the slotted eccentric SPM machines.

At first, the PMs' arrangement on the rotor is equalized by an ESC at the rotor surface. This task is carried out by providing the condition of H_1, i.e. applying the equality condition between the tangential fields at $r=R_m$ in the slotless concentric machines shown in Fig.2 (a) and (b). In the second step, by applying H_2 the concentric slotless stator is removed and replaced with the slotted and eccentric stator as shown in Fig.2 (d). Consequently, the Poisson equation in the machine in Fig.2 (c) is equalized with the Laplace equation in the machine in Fig.2 (d). At this point CTs could be applied to solve the problem of Fig.2 (d) with no concern about magnet deformation or the type of PM magnetization pattern, M. In the proposed model all PM magnetization patterns could be considered. Hereafter, by using this hypothesis and applying some CTs the field distribution of the eccentric slotted SPM machine (Fig.2 (c) and (d)) is obtained.

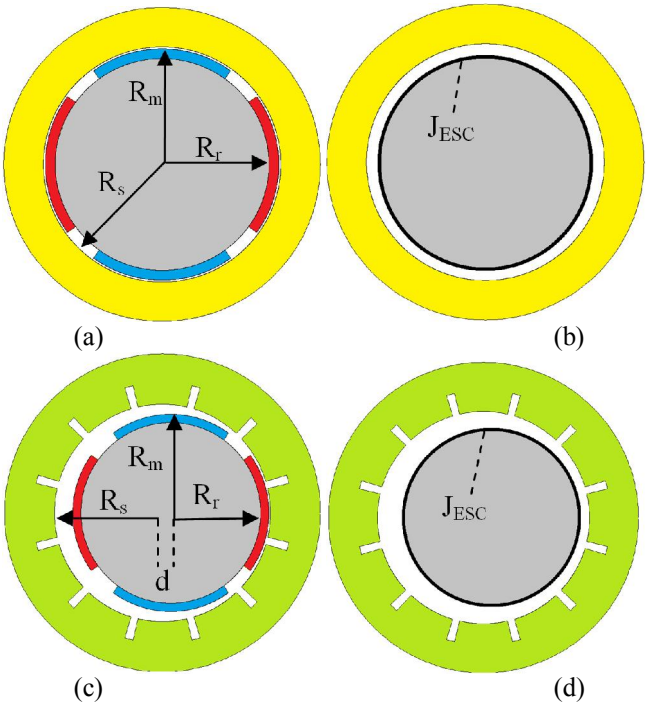

Fig. 2. (a) Slotless machine with PMs, (b) slotless machine with ESC, (c) slotted machine with PMs, (d) slotted machine with ESC.

III. Modeling

As described in the section II, at first the ESC on the rotor surface in Fig.2 (b) is obtained by applying H_1. This ESC could be obtained for PMs with any magnetization patterns. For this purpose, the field distribution of PMs in Fig.2 (a) and the flux density of ESC in Fig.2 (b) are obtained analytically and the equality condition between the obtained tangential fields at $r=R_m$ is imposed.

A. PM flux density

To find the magnetic flux distribution of PMs in Fig.2 (a), two regions are defined as (1), where R_s and R_r is the stator and rotor radius, respectively.

$$\text{I:PM } R_r < r < R_m,\ \text{II:air } R_m < r < R_s \tag{1}$$

The governing equation on the region I and II is given in (2).

$$\nabla^2 A_{I-PM} = -\mu_0 \nabla \times \mathbf{M} = \frac{1}{r}\left(\partial \frac{rM_\varphi}{\partial r} - \partial \frac{M_r}{\partial \varphi_r}\right)$$
$$\nabla^2 A_{II-PM} = 0 \tag{2}$$

where, μ_0 is the free space permeability, r and φ_r are the radial and circumferential variables in the rotor reference frame, **M** is the PM magnetization, A is the axial component of the magnetic potential vector and M_r and M_φ are the radial and circumferential components of **M**. The Fourier coefficients of M_r and M_φ for different magnetization patterns are given in [7]. The boundary conditions are expressed in (3).

$$\left.\frac{\partial A_{I-PM}}{\partial r}\right|_{R=R_r} = -\mu_0 M_\varphi,\quad \left.\frac{\partial A_{II-air}}{\partial r}\right|_{R=Rs} = 0$$
$$\left.\frac{\partial A_{II-PM}}{\partial r}\right|_{R=R_m} - \left.\frac{\partial A_{I-PM}}{\partial r}\right|_{R=R_m} = -\mu_0 M_\varphi, \tag{3}$$
$$\left.\frac{\partial A_{II-PM}}{\partial \varphi_r}\right|_{R=R_m} = \left.\frac{\partial A_{I-PM}}{\partial \varphi_r}\right|_{R=R_m}$$

The circumferential field in the region II is obtained by using the separation of variables method, as (4).

$$B_{\varphi II-PM} = \sum a_n \left(r^{np-1} - R_s^{2np} r^{-np-1}\right) \sin np\left(\varphi_r - \theta_r\right) \tag{4}$$

where, p is the number of the machine pole pairs, and θ_r is the rotor angular position and,

This article has been accepted for publication in a future issue of this journal, but has not been fully edited. Content may change prior to final publication. Citation information: DOI 10.1109/TMAG.2017.2748501, IEEE Transactions on Magnetics

$$a_n = \eta_n k_n + \frac{\mu_0 M_{\varphi n}}{2np}\left(2R_r^{np+1} - R_m^{-np+1}R_r^{2np} - R_m^{np+1}\right)$$

$$k_n = \begin{cases} -\mu_0 \dfrac{M_{r1} + M_{\varphi 1}}{2}\ln r & np = 1 \\ \mu_0 \dfrac{M_{\varphi n} + npM_m}{(np)^2 - 1} & np \neq 1 \end{cases} \quad (5)$$

$$\eta_n = \frac{R_r^{np+1}}{np} + \left[\frac{np-1}{2np} - 1\right] R_r^{2np} R_m^{-np+1} + \frac{np-1}{2np} R_m^{np+1}$$

B. ESC flux density

To find the magnetic flux distribution of the ESC in Fig. 2 (b) one region is defined as (6).

$$\text{III:air } R_r < r < R_m \quad (6)$$

The governing equation on the region III and the boundary conditions of the problem in Fig.2 (b) are given in (7) and (8), respectively, where, J_{ESC} is the current density of the ESC and presented in the form of the Fourier series in (9).

$$\nabla^2 A_{III-ESC} = 0 \quad (7)$$

$$\left.\frac{\partial A_{III-ECS}}{\partial r}\right|_{R=R_r} = \mu_0 J_{ECS}, \quad \left.\frac{\partial A_{III-ECS}}{\partial r}\right|_{R=Rs} = 0 \quad (8)$$

$$J_{ESC}(\varphi_r) = \sum_{n=1,\ldots} J_{cnESC}\cos np\varphi_r + J_{snESC}\sin np\varphi_r \quad (9)$$

Using the separation of variable method and applying (8) and (9) in (7), the circumferential field component caused by the ESC is computed as (10).

$$B_\varphi(\varphi_r) = \sum_{n=1,3,\ldots} (r^{np-1} - R_s^{2np} r^{-np-1})(c_n \cos np\varphi_r + d_n \sin np\varphi_r) \quad (10)$$

where,

$$(c_n, d_n) = \frac{\mu_0}{(R_r^{np-1} - R_s^{2np} R_r^{np-1})}(J_{ESCcn}, J_{ESCsn}) \quad (11)$$

C. Finding ESC

Based on H_1, to have the same field distribution in the region II in Fig.2 (a) and (b), the same tangential flux density must be produced by PMs and ESC at $r=R_m$. Applying the equality condition between (4) and (10) will result in (12) for the Fourier coefficients of the ECS.

$$(J_{ESCcn}, J_{ESCsn}) = \sigma_n(-\sin\theta_r, \cos\theta_r)$$
$$\sigma_n = \frac{a_n}{\mu_0}(R_r^{np-1} - R_s^{2np} R_r^{np-1})(R_m^{np-1} - R_s^{2np} R_m^{-np-1}) \quad (12)$$

By considering (9) and (12) as the ECS and applying H_2, there is an equality condition for the field distribution in the air gap region of Fig.3 (c) and (d). Hereafter, the eccentric slotted SPM machine with ESC in Fig.2 (d) is studied instead of the eccentric slotted SPM machine in Fig.2 (c).

D. Conformal transformations

The governing equation on the slotted machine with ESC in Fig.2 (d) is in the form of the Laplace equation and CTs could be applied with no concerns about the PM deformation or the PM magnetization pattern. The plane of the geometry of Fig.2 (d) is named as the S-plane and shown in Fig.3 (a). A sequence of CTs is applied to convert the slotted eccentric machine in Fig.3 (a) to a concentrated slotless one in Fig.3 (e). The target contour for computation of the flux density is a circle in the air gap which is concentric with the stator and illustrated in Fig.3 by the dotted line. At first, the eccentric geometry in the S-plane, is transformed to the concentric geometry in the T-plane, see Fig.3 (b), by using the given bilinear transformation in (13), where d is the value of the rotor eccentricity.

$$t(s) = \frac{s + fR_s}{fs + R_s}, \quad s(t) = \frac{-R_s t + fR_s}{ft - 1}$$
$$f = \frac{-U + \sqrt{U^2 - 4}}{2}, U = \frac{-R_r^2 + d^2 + R_s^2}{dR_s} \quad (13)$$

It is expected that the obtained slotted SPM machine in the T-plane is concentric and its stator has unequal teeth. In this step it is assumed that the slot lateral sides in the T-plane have constant angles with infinite length. This assumption is just for simplification of using the next CT and causes no error in the field computation. Considering this assumption, and applying the CT in (14) on the geometry in the T-plane, the machine geometry in the W plane is obtained, as shown in Fig.3 (c).

$$w(t) = \ln(t), \quad t(w) = e^W \quad (14)$$

The next used CT is in the form of Schwartz-Christofell as (15). This CT and its inverse are applied by using the Schwartz-Christofell toolbox developed for the MATLAB users [26]. Applying (15), the geometry shown in Fig.3 (d) in the Z-plane is obtained.

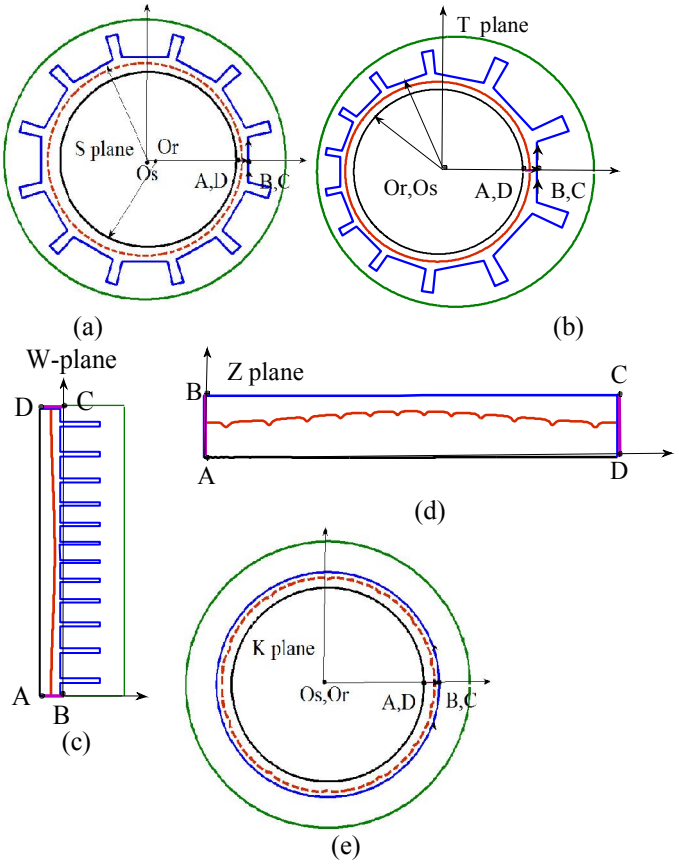

Fig. 3. The geometry of the machine with ESC in the (a) S-plane, (b) T-plane, (c) W-plane, (d) Z-plane, and (e) K-plane with slotless geometry

This article has been accepted for publication in a future issue of this journal, but has not been fully edited. Content may change prior to final publication. Citation information: DOI 10.1109/TMAG.2017.2748501, IEEE Transactions on Magnetics

TABLE I
PARAMETERS OF THE CONSIDERED SPM MACHINES.

parameter	Symbol	Machine No.1	Machine No.2
pole pairs	p	2	2
Stator bore	R_s	60 mm	70 mm
Air gap length	g	1 mm	1 mm
Rotor radius	R_r	54 mm	64 mm
PM arc angle	$\alpha\tau_p$	72°	80°
PM remanent flux density	B_{rem}	1.2 T	1.2 T
Machine stack length	L_{stk}	100 mm	50 mm
Eccentricity	d	0.8 mm	0.7 mm
Slot opening (mech. deg.)	b_o	4.8°	4°
No. of the stator slots	Q_s	12	6

$$z(w) = A\int\prod_{k=1}^{n-1}(w - w_k)^{-\frac{\alpha_k}{\pi}-1}dw + C \tag{15}$$

The last used CT maps the Z-plane to K-plane by (16).

$$k(z) = e^{\frac{2\pi}{u_1}\left(z^* - \frac{v_1}{2}\right)-\frac{\pi}{j}}$$
$$z(k) = \frac{u_1}{2j}\left(-1 + j\frac{\ln(k)}{\pi}\right) + \frac{v_1}{2} \tag{16}$$

where, u_1 and v_1 are the length of the lines BC and CD in Fig.3 (d), and the superscript * denotes for complex conjugation. The resulted geometry in the K-plane, Fig.3 (e), is a slotless machine. The governing equation and the boundary condition in the K-plane is as (17) and (18), respectively.

$$\nabla^2 A^K_{ESC} = 0 \tag{17}$$

$$\left.\frac{\partial A^K_{ECS}}{\partial r^K}\right|_{r^K = R_r^K} = \mu_0 J^K_{ECS}\ ,\quad \left.\frac{\partial A^K_{ECS}}{\partial \varphi_r^K}\right|_{R = R_S^K} = 0 \tag{18}$$

where, the superscript K shows the related variables are expressed in the K-plane. The J^K_{ESC} is considered as the boundary condition and is obtained by applying the introduced CTs on the J_{ESC} as (19) [24].

$$J^K_{ECS} = J_{ECS}\left(\frac{ds}{dt}\right)^*\left(\frac{dt}{dw}\right)^*\left(\frac{dw}{dz}\right)^*\left(\frac{dz}{dk}\right)^* \tag{19}$$

where, "*" denotes for the complex conjugation operator. It is worth mentioning that, to apply (19), the ESC in (9) is made discrete to N_s number of discrete values as (20).

$$J_{ESC}(x, y) = \sum_{i=1}^{N_s} J_{i-ESC}$$
$$J_{i-ESC} = \begin{cases} J_{ESC}(x_i, y_i) & \text{at the i}^{\text{th}}\text{ segment} \\ 0 & \text{elsewhere} \end{cases} \tag{20}$$

The point (x_i,y_i) in the S-plane is mapped to the point (u_i,v_i) in the K-plane by applying (13)-(16). In addition, the current density of the i^{th} segment in point (x_i,y_i) in the S-plane is transferred to the point (u_i,v_i) in the K-plane by value reported in (19). The width of the i^{th} segment in the S-plane is $2\pi R_s/N_s$. The width of the map of the i^{th} segment in the K-plane is expressed as γ_i^K. The Fourier representation of J^K_{ESC} in the i^{th} segment in the K-plane is expressed in (21), where υ is the angular position in the K-plane.

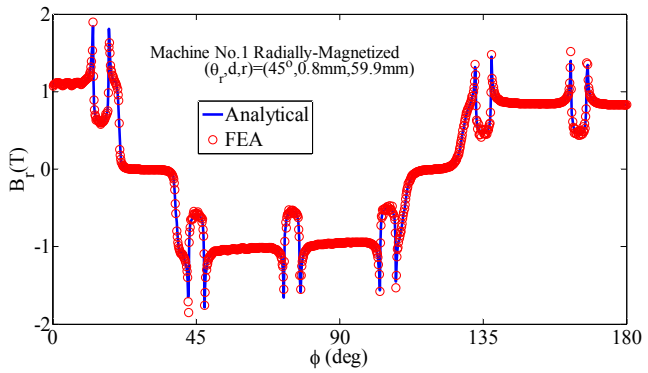

(a)

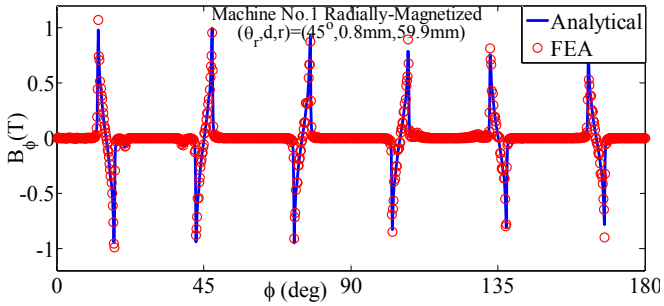

(b)

Fig. 4. The air gap flux density for the machines no.1 for radially magnetized PMs and θr=45°(a) radial and (b) circumferential component

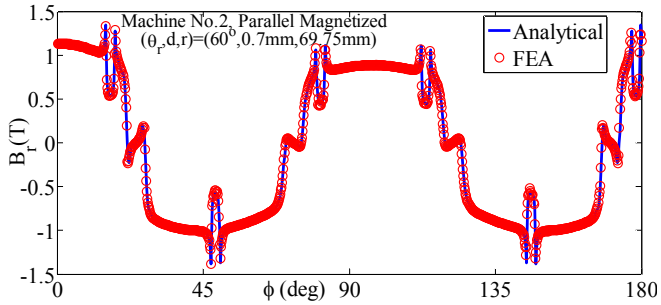

(a)

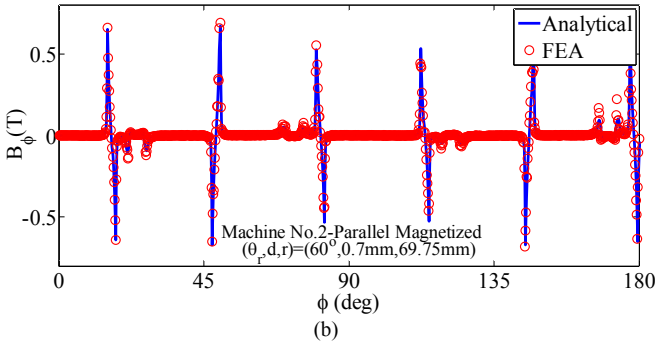

(b)

Fig. 5. The air gap flux density for the machines no.2 for parallel-magnetized PMs and θr=60°(a) radial and (b) circumferential component

This article has been accepted for publication in a future issue of this journal, but has not been fully edited. Content may change prior to final publication. Citation information: DOI 10.1109/TMAG.2017.2748501, IEEE Transactions on Magnetics

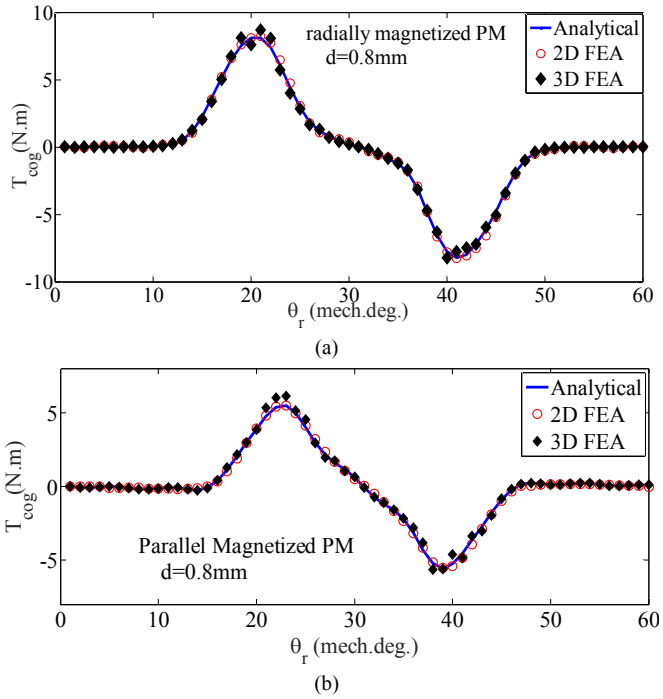

Fig. 6. Cogging torque for the machine no.1 with (a) radially- and (b) parallel magnetized PMs.

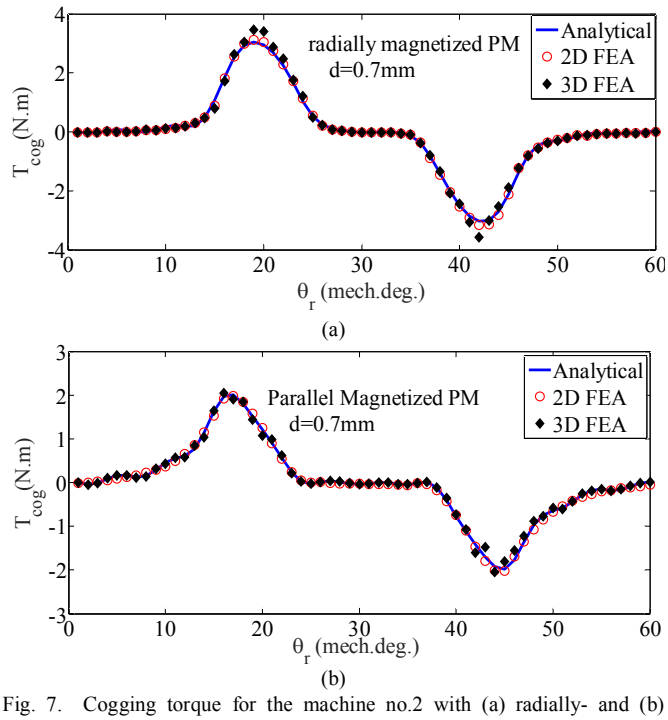

Fig. 7. Cogging torque for the machine no.2 with (a) radially- and (b) parallel magnetized PMs.

$$J_{ESC}^{K}(\upsilon)=\sum_{n}^{\infty}J_{ESCsn}^{K}\sin(n\upsilon)+J_{ESCcn}^{K}\cos(n\upsilon)$$

$$J_{ESCsn}^{K}=\sum_{i=1}^{N_s}\zeta_i\left[\cos(n\upsilon_{i-})-\cos(n\upsilon_{i+})\right] \quad (21)$$

$$J_{ESCcn}^{K}=\sum_{i=1}^{N_s}\zeta_i\left[\sin(n\upsilon_{i+})-\sin(n\upsilon_{i-})\right]$$

$$\upsilon_{i-}=\upsilon_i-\frac{\gamma_i^K}{2},\upsilon_{i+}=\upsilon_i+\frac{\gamma_i^K}{2},\zeta_i=\frac{J_{iESC}^{K}}{2n\pi}$$

Using the separation of variables method and considering (18), the magnetic field components in the K-plane are obtained as (22), where ρ is the radial variable in the K-plane.

$$B_{\rho}^{K}=\sum_{n}\tau_n\left(J_{ESCcn}^{K}\sin(n\upsilon)-J_{ESCsn}^{K}\cos(n\upsilon)\right)$$
$$B_{\upsilon}^{K}=\sum_{n}\tau_n\left(J_{ESCsn}^{K}\sin(n\upsilon)+J_{ESCcn}^{K}\cos(n\upsilon)\right) \quad (22)$$
$$\tau_n=\mu_0\frac{\rho^{n-1}+\rho_s^{2n}\rho^{-n-1}}{\rho^{n-1}-\rho_s^{2n}\rho_r^{-n-1}}$$

Therefore the solution of the magnetic field in the S-plane for the eccentric slotted SPM machine in Fig.2 (d) could be easily obtained by coming back from the K-plane to the S-plane as the procedure explained in (23).

$$\mathbf{B}^{\mathbf{K}}=B_{\rho}^{K}\mathbf{a}_{\rho}^{\mathbf{K}}+B_{\upsilon}^{K}\mathbf{a}_{\upsilon}^{\mathbf{K}}=B_{x_K}^{K}+jB_{y_K}^{K}$$
$$\mathbf{B}^{\mathbf{S}}=\frac{\mathbf{B}^{\mathbf{K}}}{\left(\frac{ds}{dt}\right)^{*}\left(\frac{dt}{dw}\right)^{*}\left(\frac{dw}{dz}\right)^{*}\left(\frac{dz}{dk}\right)^{*}} \quad (23)$$

where $\mathbf{a}^{\mathbf{K}}_{\rho}$ and $\mathbf{a}^{\mathbf{K}}_{\upsilon}$ are the radial and circumferential unitary vectors in the K-plane, respectively.

E. Cogging torque and UMF

The Maxwell stress tensor is used to compute the machine cogging torque as given in (24).

$$T=\frac{r^2L_{stk}}{\mu_0}\int_0^{2\pi}B_rB_{\varphi_r}d\varphi_r \quad (24)$$

where, B_r and $B_{\varphi r}$ are the radial and circumferential components of the air gap flux density in the considered Maxwell surface in the S-plane, r is the radius of the considered Maxwell surface and L_{stk} is the machine stack length.

The x- and y- components of the UMF are predicted by (25).

$$F_x=\frac{rL_{stk}}{2\mu_0}\int_0^{2\pi}B_g^2\cos\varphi_r d\varphi_r$$
$$F_y=\frac{rL_{stk}}{2\mu_0}\int_0^{2\pi}B_g^2\sin\varphi_r d\varphi_r \quad (25)$$

where, B_g is the magnitude of the air gap flux density in the points of the considered Maxwell surface in the S-plane.

IV. Model Verification

To verify the proposed model, the analytically obtained results are compared with FEA for two SPM machines. The FEA is carried out by FEMM software [28]. Parameters of the considered SPM machines are reported in Table 1. Both radially- and parallel-magnetized PMs, are studied.

This article has been accepted for publication in a future issue of this journal, but has not been fully edited. Content may change prior to final publication. Citation information: DOI 10.1109/TMAG.2017.2748501, IEEE Transactions on Magnetics

The predicted magnetic flux density components in the machine No.1 in θ_r=45° for radially-magnetized PMs are shown and compared with FEA results in Fig.4 (a) and (b). The magnetic flux density components in the machine No.2 with parallel-magnetized PMs in θ_r=60° are shown and compared with FEA results in Fig.5 (a) and (b). The FEA and analytically obtained results for cogging torque of the machines No.1 and the machine No.2 with radially- and parallel magnetized PMs are illustrated in Fig.6 and Fig.7, respectively. The UMF components in the considered machines with radially and parallel magnetized PMS are shown in Fig. 8 and Fig.9, respectively. As seen in Fig.8 (c) and (d), there is some small and negligible fluctuation in the computed y component of UMF. This fluctuation could be due to the discrete format of the ESC, as well as the tolerances in computations of the Schwartz-Christofell toolbox. However the error percentage in the magnitude UMF is negligible. As shown in Fig. (4)-(9), the model results are in a good agreement with FEA.

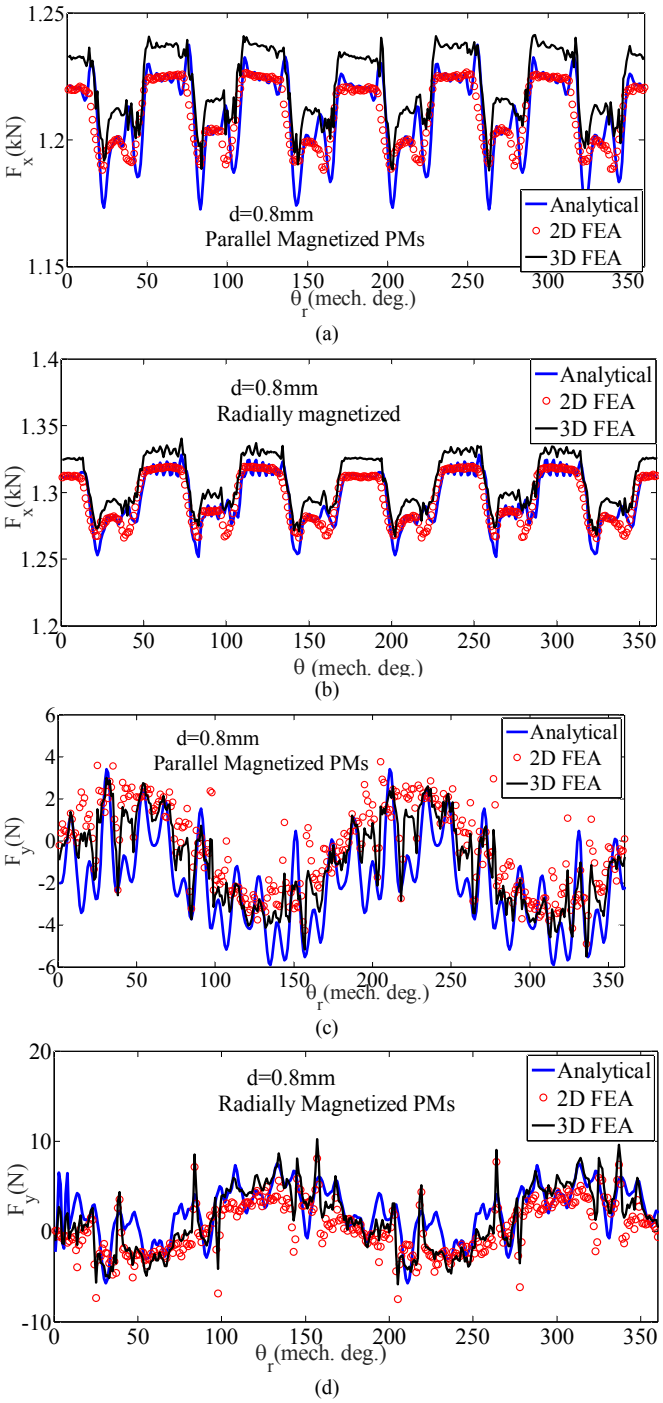

Fig. 8. The components of UMF for the machine No.1. F_x for (a) parallel and (b) radially- magnetized PMs. F_y for (c) parallel and (d) radially-magnetized PMs.

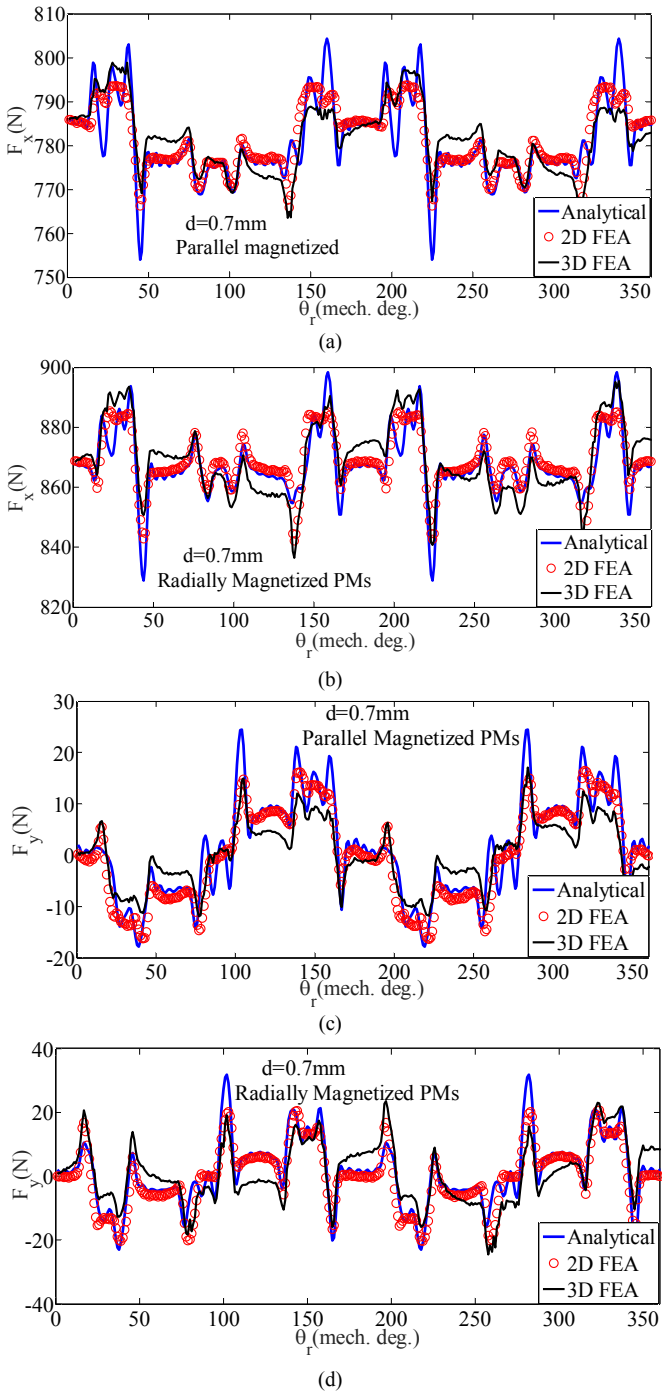

Fig. 9. The components of UMF for the machine No.2. F_x for (a) parallel and (b) radially- magnetized PMs. F_y for (c) parallel and (d) radially-magnetized PMs.

V. Conclusion

In this work an analytical approach is proposed for modeling of the slotted eccentric SPM machines. In the developed model the PMs' arrangement is replaced with an ESC on the rotor surface. By this trick, the governing equation is converted from Poisson to Laplace equation. Therefore, applying the CTs is carried out with no concerns about the PM deformation. The main source of inaccuracy in the previous studies with conformal transformations was neglecting the PM deformation. Thanks to the ESC, the inaccuracy and the limitation of the previous models are removed and the obtained results have a good agreement with FEA. The model is approved by comparing the results of cogging torque and the produced UMF with FEA.

VI. Acknowledgment

This research is supported by the grant number 94GRD1M930 of the Shahrekord University, Shahrekord, Iran.

References

[1] S. M. Hwang, J. B. Eom, G.-B. Hwang, W.-B. Jeong, and Y.-H. Yung, "Cogging torque and acoustic noise reduction in permanent magnet motors by teeth pairing," *IEEE Trans. Magn.*, vol. 36, no. 5, pp. 3144–3146, Sep. 2000.

[2] Z. Q. Zhu, Z. P. Xia, L. J. Wu, and G. W. Jewell, "Influence of slot and pole number combination on radial force and vibration modes in fractional slot PM brushless machines having single-and double layer windings," in Proc. IEEE Energy Convers. Congr. Expo. (ECCE), Sep. 2009, pp. 3443–3450.

[3] H. Yang, Y. Chen, "Influence of Radial Force Harmonics With Low Mode Number on Electromagnetic Vibration of PMSM," *IEEE Trans. Energy Convers.*, vol.29. no.1, Mrch 2014, pp. 38-45.

[4] G. Verez, G. Barakat, Y. Amara, and G. Hoblos, " Impact of Pole and Slot Combination on Vibrations and Noise of Electromagnetic Origins in Permanent Magnet Synchronous Motors," IEEE Trans. Magn., vol. 51, no. 3, March 2015, pp. 8101104.

[5] H. J. Shin, J. Y. Choi, H. I Park, and S. M. Jang, "Vibration Analysis and Measurements Through Prediction of Electromagnetic Vibration Sources of Permanent Magnet Synchronous Motor Based on Analytical Magnetic Field Calculations," IEEE Trans. Magn., Vol. 48, no. 11, Nov. 2012, pp.4216-4219.

[6] D. Zarko, D. Ban, and T. Lipo, "Analytical solution for cogging torque in surface permanent-magnet motors using conformal mapping," *IEEE Trans. Magn.*, vol. 44, no. 1, pp 52-65, January 2008.

[7] K. Boughrara, B. L. Chikouche, R. Ibtiouen, D. Zarko, and O. Touhami, "Analytical Model of Slotted Air-Gap Surface Mounted Permanent-Magnet Synchronous Motor With Magnet Bars Magnetized in the Shifting Direction," IEEE Trans. Magn., vol. 45, no. 2, Feb. 2009, pp. 747-758

[8] S. Taghipour, A. Abedini, A. Oraee and H. Oraee, "Approach for analytical modeling of axial-flux PM machines," *Proc. IET-EPA*, vol.10, no.10, Jul. 2016, pp. 441-450.

[9] L. J. Wu, Z. Q. Zhu, D. Staton, M. Popescu, and D. Hawkins, "An Improved Subdomain Model for Predicting Magnetic Field of Surface-Mounted Permanent Magnet Machines Accounting for Tooth-Tips," IEEE Trans. Magn., VOL. 47, NO. 6, JUNE 2011 1693-1704.

[10] D. Lin, S. L.Ho, and W. N. Fu, "Analytical prediction of cogging torque in surface-mounted permanent-magnet motors," *IEEE Trans. Magn.*, vol. 45, no. 9, pp 3296-3302, Sep 2009.

[11] S. Taghipour, and V. Zamani, 'A Novel Analytical Model for No-Load, Slotted, Surface-Mounted PM Machines: Air gap Flux Density and Cogging Torque', IEEE Trans. Magn., vol.51, no. 4, 2015, pp. 8104008

[12] K. J. Binns, P. J. Lawrenson, C. W. Trowbridge, The Analytical and Numerical Solution of Electric and Magnetic Fields, John Wiley

[13] L.J. Wu, Z.Q. Zhu, D. Staton, M. Popescu, D. Hawkins, "Comparison of analytical models of cogging torque in surface-mounted PM machines," *IEEE Trans. on Ind. Electron.*, vol.59. no.6, pp.2414-2425, 2012.

[14] U. Kim and D. K. Lieu, "Magnetic Field Calculation in Permanent Magnet Motors with Rotor Eccentricity: With Slotting Effect Considered," IEEE Trans. Magn., vol. 34, no. 4, July 1998, pp. 2253-2266.

[15] J. Fu and C. Zhu, Subdomain Model for Predicting Magnetic Field in Slotted Surface Mounted Permanent-Magnet Machines With Rotor Eccentricity, IEEE Trans. Magn., vol. 48, no. 5, May 2012, pp. 1906-1917.

[16] L. Gasparin, A. Cernigoj, S. Markic, and R. Fiser, "Additional cogging torque components in permanent-magnet motors due to manufacturing imperfections," IEEE Trans. Magn., vol. 45, no. 3, pp. 1210–1213, Mar. 2009.

[17] H. Qian, H. Guo, Z. Wu, and X. Ding, "Analytical Solution for Cogging Torque in Surface-Mounted Permanent-Magnet Motors With Magnet Imperfections and Rotor Eccentricity," IEEE Trans. Magn., vol. 50, no. 8, Aug. 2014 pp. 8201615.

[18] Y. Li, Q. Lu, Z. Q. Zhu, L. J. Wu, G. J. Li, and D. Wu, "Analytical Synthesis of Air-Gap Field Distribution in Permanent Magnet Machines With Rotor Eccentricity by Superposition Method," IEEE Trans. Magn., vol. 51, no. 11, pp. 8110404, Nov. 2015.

[19] J. T. Li, Z. J. Liu, and L. H. A. Nay, "Effect of radial magnetic forces in permanent magnet motors with rotor eccentricity," IEEE Trans. Magn., vol.43,no.6,pp.2525–2527,Jun.2007.

[20] F. R. Alam, K. Abbaszadeh, "Magnetic Field Analysis in Eccentric Surface-Mounted Permanent-Magnet Motors Using an Improved Conformal Mapping Method", IEEE Trans. Energy Convers., vol.31, no.1, Nov.2015, pp.1-12.

[21] Y. Huanga, B. Guoa, Y. Guob, J. Zhub, A. Hemeidac and P. Sergeant, "Analytical modeling of axial flux PM machines with eccentricities," Int. J. Appl. Elect. and Mech., vol. 53, 2017, pp.757–777.

[22] Y. Huanga, B. Guoa, A. Hemeidac and P. Sergeant, "Analytical modeling of static eccentricities in axial flux PM machines with Concentrated Windings," Energies, vol. 9, 2016, doi:10.3390/en9110892.

[23] P. Jalali, S. T. Boroujeni, and N. Bianchi, 'A simple and efficient model for slotless eccentric surface-mounted PM machines," *Proc. IET-EPA*, vol.11, no.4, Apr. 2017, pp. 631-639.

[24] P. Jalali, S. T. Boroujeni, and Bianchi, N.: 'Analytical modeling of slotless eccentric surface-mounted PM machines using a conformal transformation', IEEE Trans. Energy Convers., vol.32, no.2, June.2017, pp. 658-666.

[25] A. Rahideh and T. Korakianitis, Analytical Open-Circuit Magnetic Field Distribution of Slotless Brushless Permanent-Magnet Machines With Rotor Eccentricity, IEEE Trans. Magn., vol. 47, no. 12, Dec. 2011, pp. 4791-4808.

[26] T. A. Driscoll, Schwarz-Christoffel Toolbox User's Guide: Version 2.3. Newark, DE: Dept. Math. Sci., Univ. Delaware, 2005.

[27] D. K. Cheng, Field and Wave Electromagnetics. Addison Wesley Publishing Company, 1983.

[28] http://www.femm.info/wiki/HomePage